Electronic Supplementary Material (ESI) for Nanoscale.
This journal is © The Royal Society of Chemistry 2018

Electronic Supplementary Information

Strain in Single-Wrinkle on MoS_2-Flake for in-Plane Realignment of Band-Structure for Enhanced Photo-Response

*Shikai Deng, Songwei Che, Rousan Debbarma and Vikas Berry**

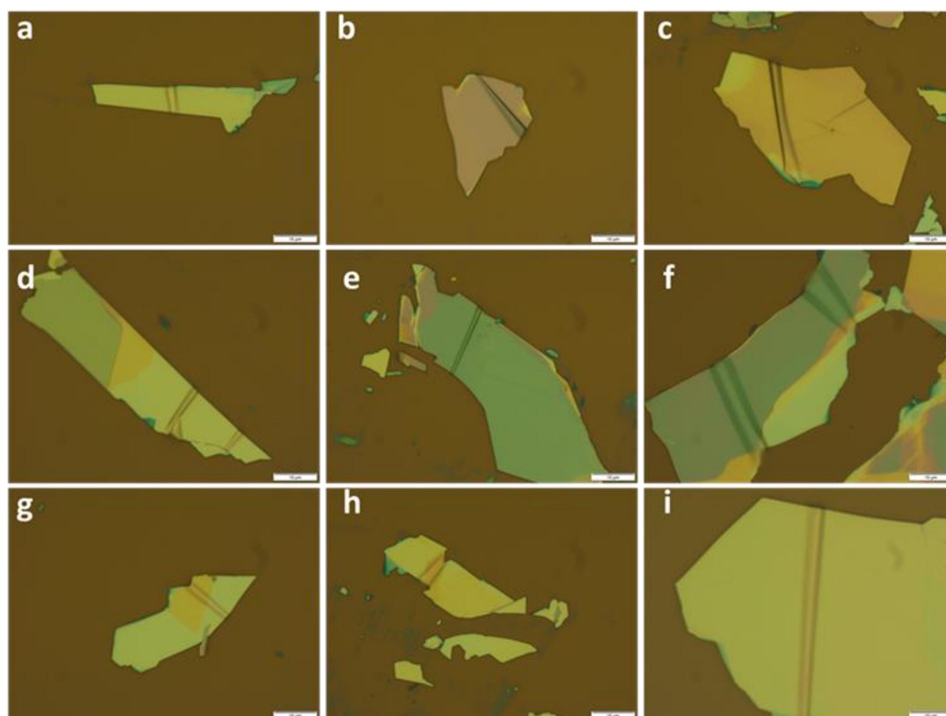

Figure S1. Optical images of some wrinkled MoS_2. Scale bars are 10μm.

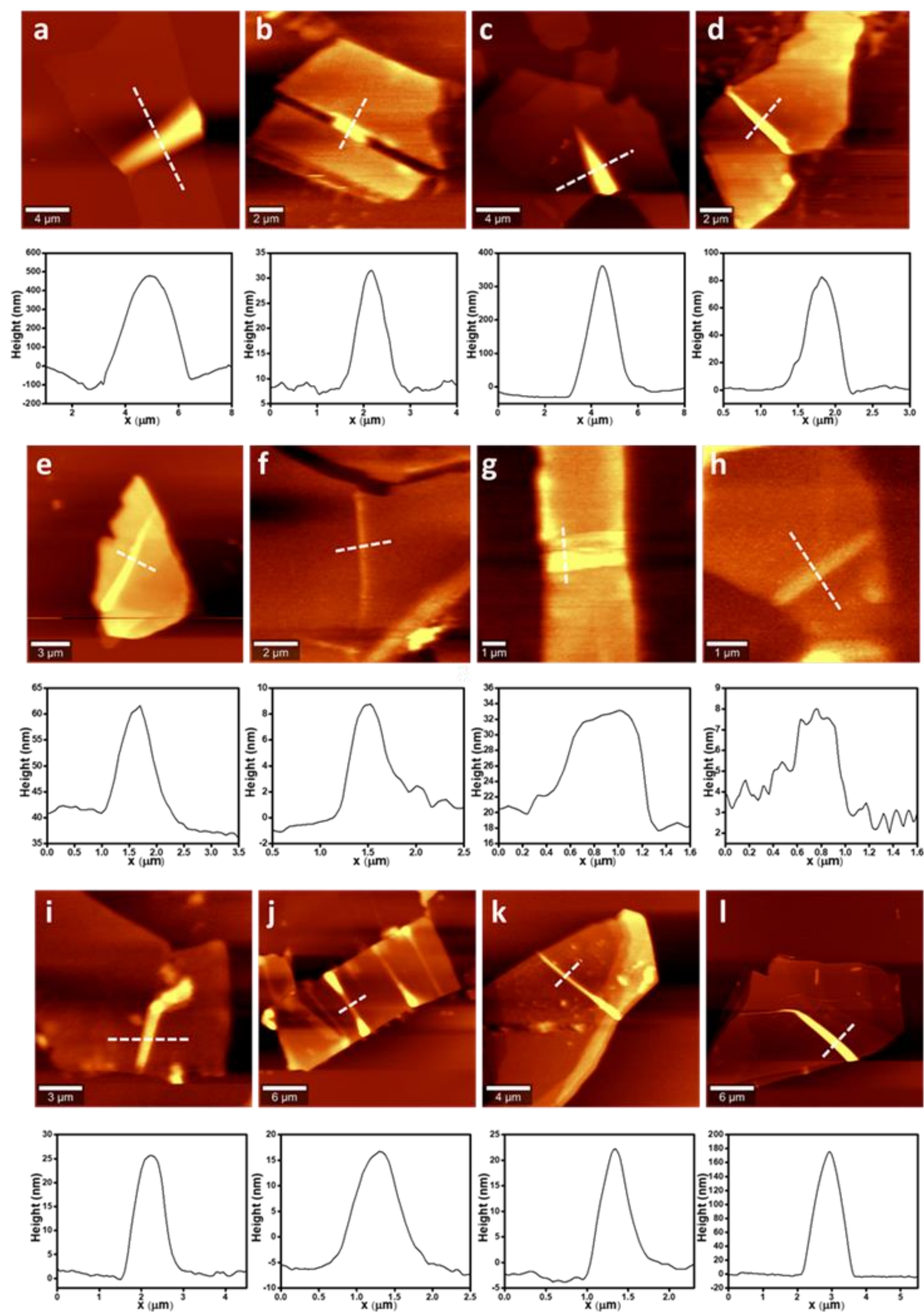

Figure S2. AFM characterization of wrinkled MoS_2 samples.

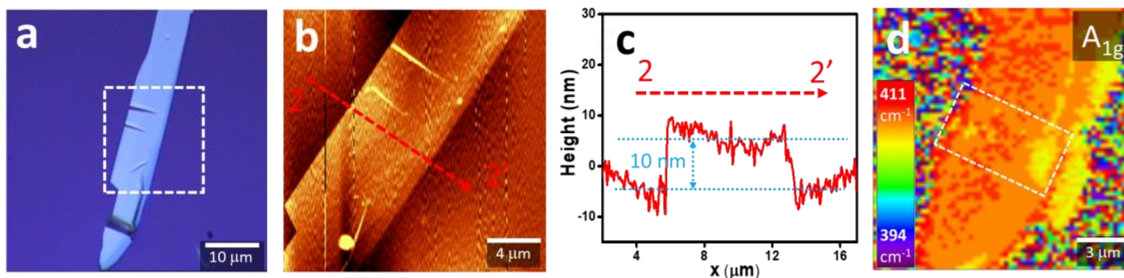

Figure S3. Wrinkled MoS_2 on SiO_2. (a) An optical image of a wrinkled MoS_2. (b) Atomic force microscopy characterization image of the wrinkled park of MoS_2 in (a). (c) Height profile of MoS_2 flake along the red dashed line (2-2') in (b). (d) Raman position mapping of A_{1g} mode.

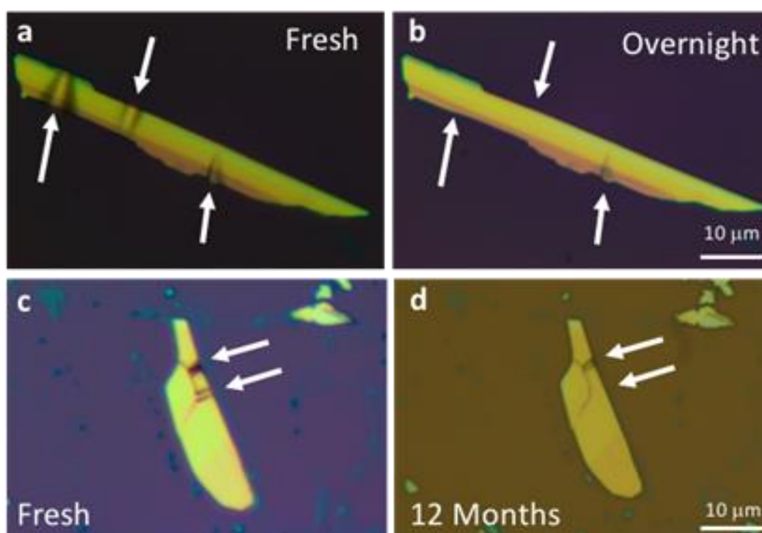

Figure S4. **Wrinkles flattening and disappearing through sliding.** (a) A fresh optical image of a wrinkled MoS_2. (b) Same MoS_2 flakes in (a) after overnight without any treatment. (c) A fresh optical image of a wrinkled MoS_2. (b) Same MoS_2 flakes in (c) after 12 months without any treatment. Arrows indicate the positions of wrinkles in fresh wrinkled MoS_2.

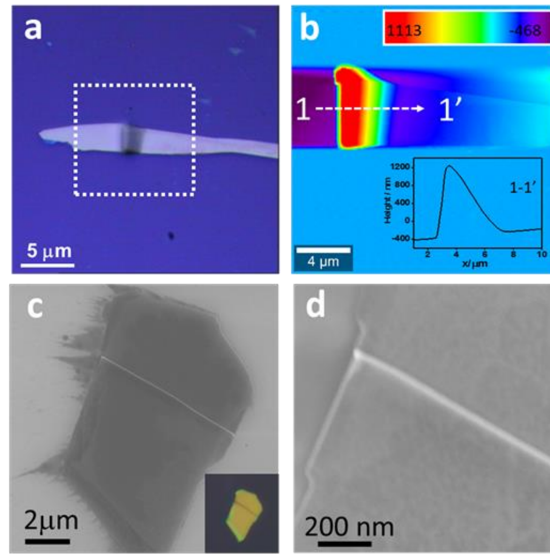

Figure S5. Asymmetric Wrinkled MoS_2 on SiO_2. (a) Optical image of an asymmetric wrinkle in MoS_2. (b) AFM characterization of the same wrinkled MoS_2 flake in (a), insert is the height profile along the dashed line (1-1'). (c) and (d) SEM characterization of an asymmetric wrinkle. Insert is the optical image of the same flake in (c).

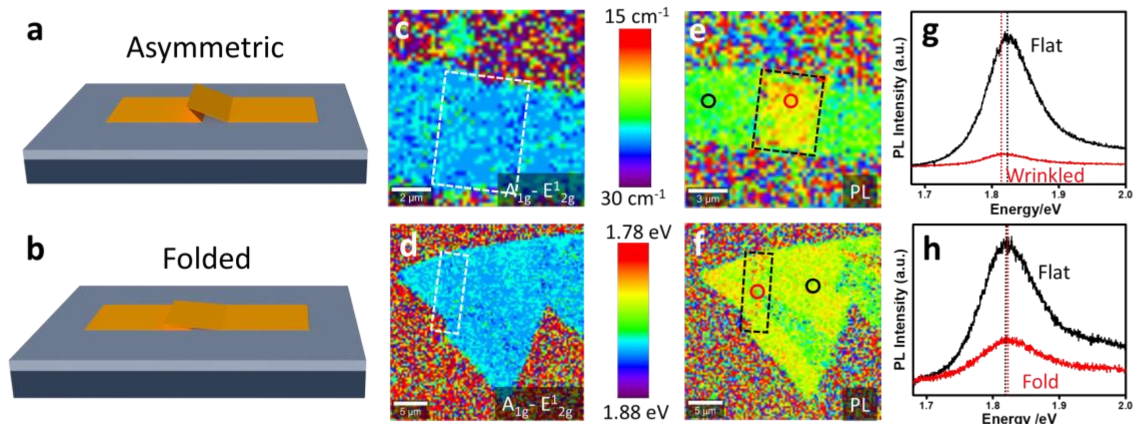

Figure S6. Raman and Photoluminescence spectroscopy of different kinds of wrinkled MoS_2. (a) to (b) Schematic of the asymmetric (a) and folded (b) wrinkles in MoS_2. (c) to (d) Raman position difference between E^1_{2g} mode and A_{1g} mode (A_{1g} - E^1_{2g}) of the asymmetric (c) and folded

(d) wrinkles in MoS_2. (e) to (f) PL energy mappings of A exciton peak for the asymmetric (e) and folded (f) wrinkles in MoS_2. The black dashed rectangles are the effected wrinkled regions. (g) to (h) PL spectra profiles measured on a flat (black) and on a wrinkled (red) regions.

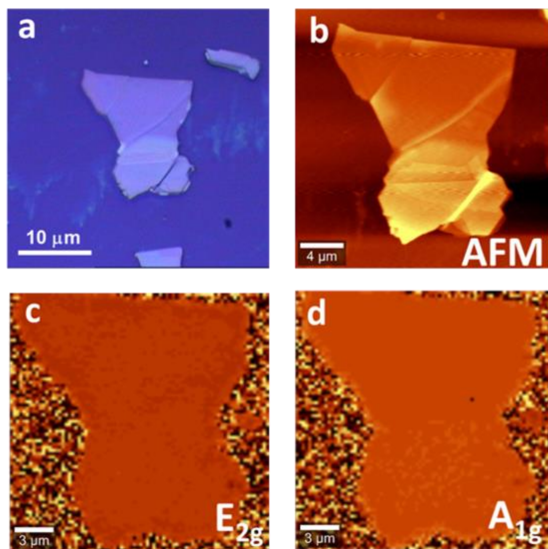

Figure S7. Small wrinkles in MoS_2 on SiO_2. (a) Optical image of a small wrinkle in MoS_2. (b) AFM characterization image of the same wrinkled in (a). (c) and (d) Raman position mapping of E^1_{2g} mode and A_{1g} mode, respectively.

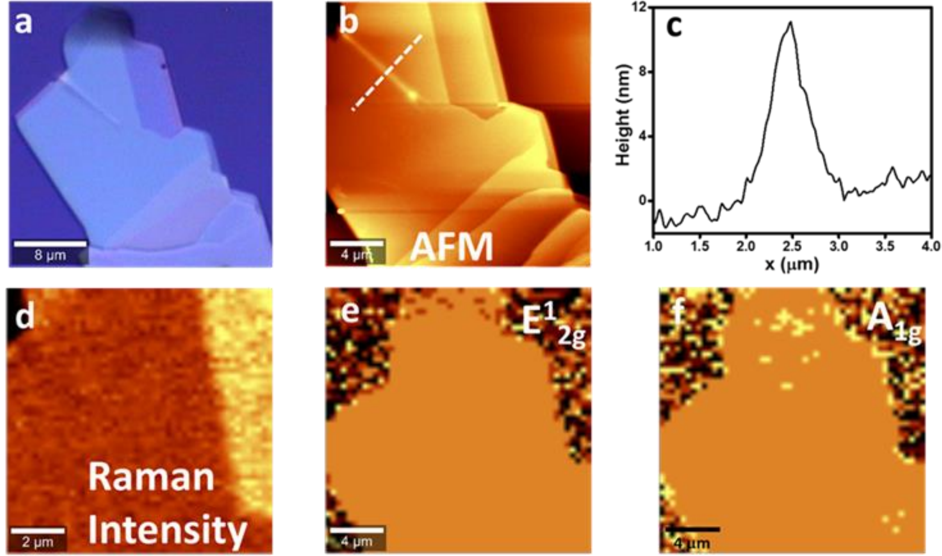

Figure S8. Small wrinkles in MoS_2 on SiO_2. (a) Optical image of a small wrinkle in MoS_2. (b) Atomic force microscopy characterization image of the same wrinkled in (a). (c) Height profile of along the dashed line in (b). (d) Raman intensity of wrinkled region in MoS_2. Raman position mapping of E^1_{2g} (e) and A_{1g} (f).

Raman and Photoluminescence versus deformation

$$\Delta = \frac{3\gamma\lambda^3}{2\pi^2 E t^3 L_p} \tag{S1}$$

The shift of E^1_{2g} peak position for this wrinkle is ~ 2 cm^{-1} as shown in Figure S2c. Plugging this into the relationship between deformation and mode position shift (2 cm^{-1}/% deformation),[1] the estimated deformation is ~ 1%. This is consistent with the deformation obtained from the Eq. 2, which is ~1.11%. The red shift of PL A peak is about 45 meV, which means the band gap reduction is about 47.6 meV/% deformation. The deformation of the wrinkle in Figure 1 is ~ 0.55 %, and the

reduction of optical band gap in this wrinkle is ~ 33.9 meV or 61 meV% deformation. More PL versus deformation data are shown in Figure S1.

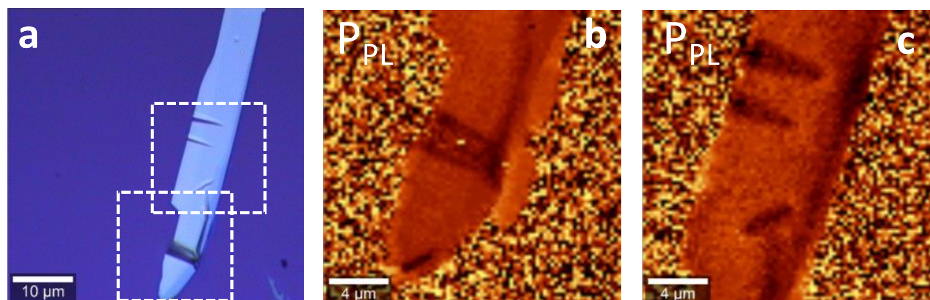

Figure S9. Wrinkled MoS_2 on SiO_2 and photoluminescence spectroscopy of wrinkled MoS_2. (a) Optical image of a MoS_2 flake with several wrinkles. (b) and (c) PL energy mappings of A exciton peak of square regions in (a). The wrinkled induced reduction of optical band gap is clear shown in (b) and (c). And the widths of band gap modified regions are much larger than the width of the wrinkles.

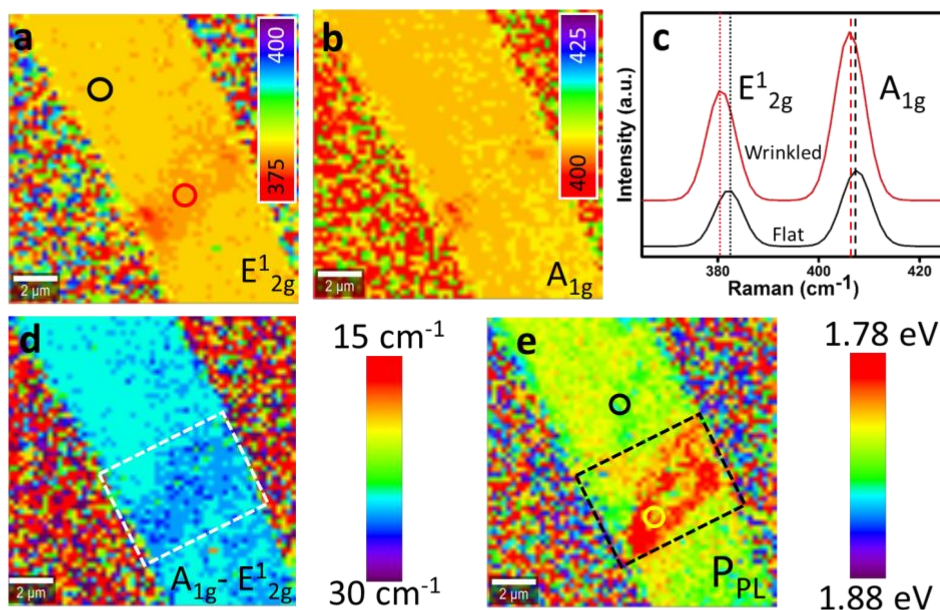

Figure S10. Raman and PL position mapping of symmetric wrinkles in MoS_2 on SiO_2. (a) and (b) Raman position mapping of E^1_{2g} mode and A_{1g} mode, respectively. The A_{1g} mode is less

affected than the E^1_{2g}. White dashed squares are wrinkled regions. The units of the scale bars in (a) and (b) are cm^{-1}. (c) Typical Raman spectra for wrinkled (red) and flat (black) MoS_2. Dotted lines and dashed lines are the positions of E^1_{2g} mode and A_{1g} mode, respectively. (d) Raman position mapping difference between E^1_{2g} mode and A_{1g} mode (A_{1g} - E^1_{2g}). White dashed rectangle is wrinkle effected region. (e) PL energy mapping of A exciton peak. Black dashed rectangle is wrinkle effected region. Note: the size characterization of this is shown a previous study.[2]

The larger red-shift of the E^1_{2g} peak than the A_{1g} peak in the wrinkled region of symmetric wrinkles leads to a slight increase in the difference between the two peaks positions (A_{1g} - E^1_{2g}). However, in asymmetrical and folded MoS_2, the difference between these two peak-positions remains nominally unchanged as shown in the A_{1g} - E^1_{2g} mappings. Although the asymmetric wrinkle (Figure S4b) shows a higher mechanical plane deformation than the symmetric one (Figure 1e), the red shift of the A peak (30 meV) in symmetric wrinkle is higher than that (10 meV) in the asymmetric one (Figure 2j, 2k). The PL peak position shows no change for the case of folded wrinkles (Figure 2l). Further, the photoluminescence-modification is localized in asymmetric wrinkles (4.5 μm, as shown in Figure 2), however, the photoluminescence is modified (4 μm) in a region 2-5 times larger than the width of symmetric wrinkle (0.8 μm), as shown in Figure 2g, S8, and S9.

Table S1 Photoluminescence versus deformation

Width (nm)	Thickness (nm)	Projection Length (nm)	Deformation (%)	PL Shift (meV)	PL Shift /Deformation (meV/%)
1157	13.9	10000	0.55	33.9	61.4
629	10.1	3620	0.63	30	47.0

526	10.6	3620	0.32	19.1	59.1
2082	19.8	30000	0.37	20	53.9
385	10	998	0.54	27.8	50.8
2206	21	10000	1.11	47.6	42.9
721	10.5	5788	0.37	25.8	48.2

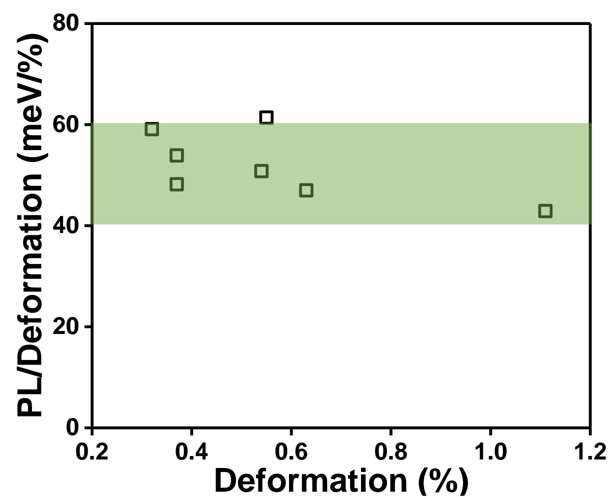

Figure S11. PL versus deformation in MoS_2 flakes.

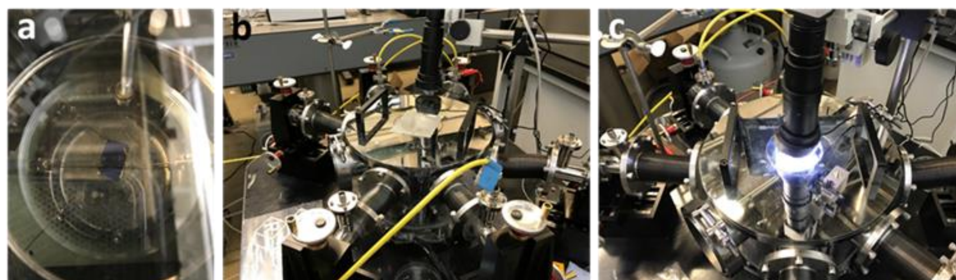

Figure S12. Electrical characterization experiment setup. (a) Electrodes Connection on the device. (b) and (c) Electrical characterization in dark and light conditions, respectively.

Additional Devices Characterization (wrinkled and flat devices on the SAME flake)

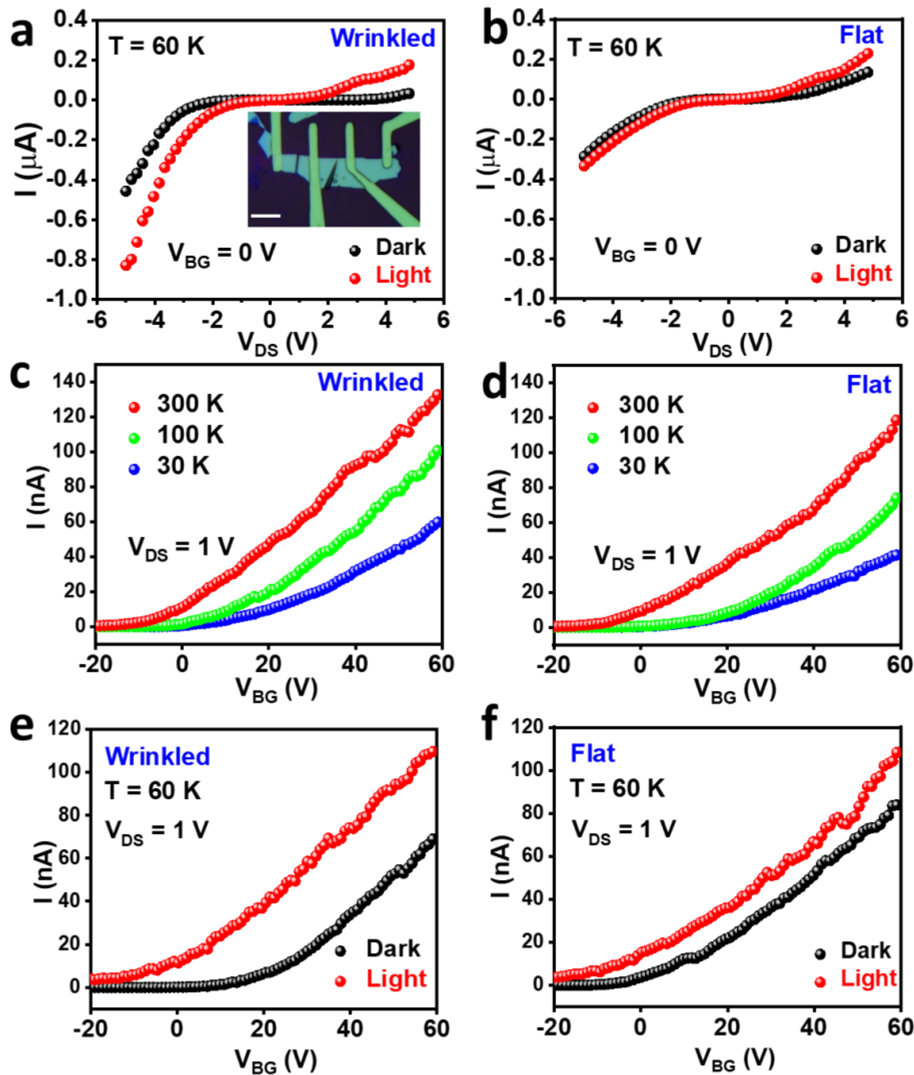

Figure S13. Device Characterization of Device 2. Source-drain current under bias of single-wrinkle (a) and flat (b) device at dark and light conditions. Scale bar in inset is 10 μm. Source-drain current in linear scale versus back gating voltage at different temperatures for single-wrinkle (c) and flat (b) MoS_2 devices. source-drain current versus back gating voltage at 60K for single-wrinkle (e) and flat devices (f).

Table S2. Photo-response of single-wrinkle and flat devices

	ON/OFF ratio				Photo-response	
	Device 1		**Device 2**		**Device 1**	**Device 2**
	Dark	Light	Dark	Light		
Flat	2.90E+04	1.80E+03	1.30E+03	2.80E+01	1.1	1.2
Wrinkled	3.80E+04	2.90E+03	3.30E+03	3.00E+01	1.5	1.8

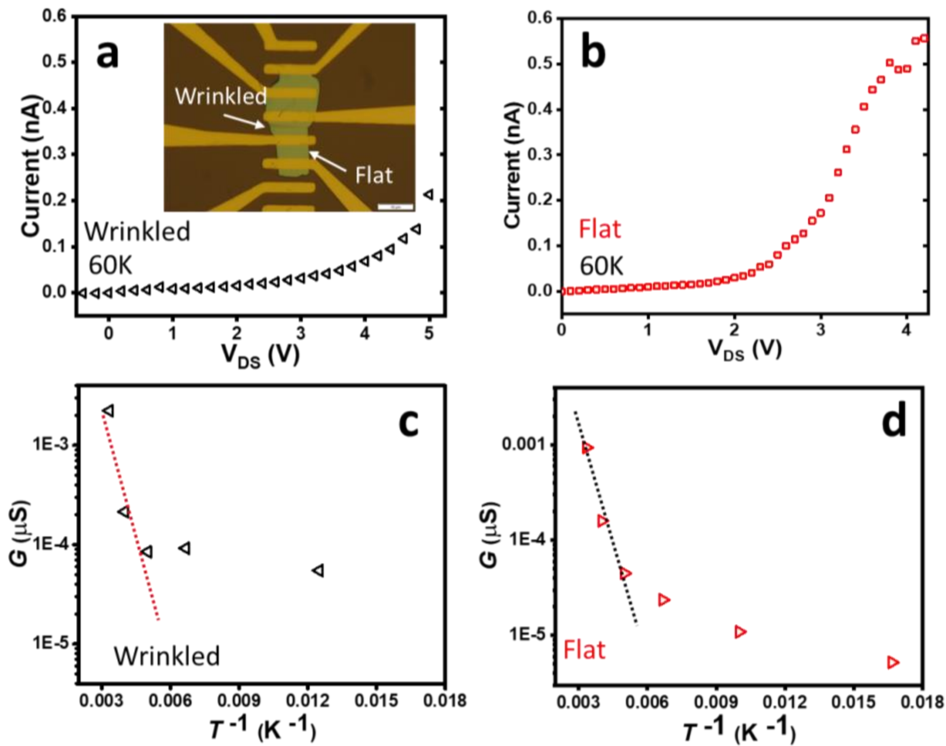

Figure S14. I_{DS}-V_{DS} (source-drain current versus source-drain voltage) characterization and temperature study of single-wrinkle and flat MoS_2 devices. (a) and (b) I_{DS} versus V_{DS} at 60K for wrinkled and flat MoS_2 devices, respectively. Data have been calibrated to exclude to instrumental errors. (c) and (d) Arrhenius plots for wrinkled and flat MoS_2 devices, respectively.

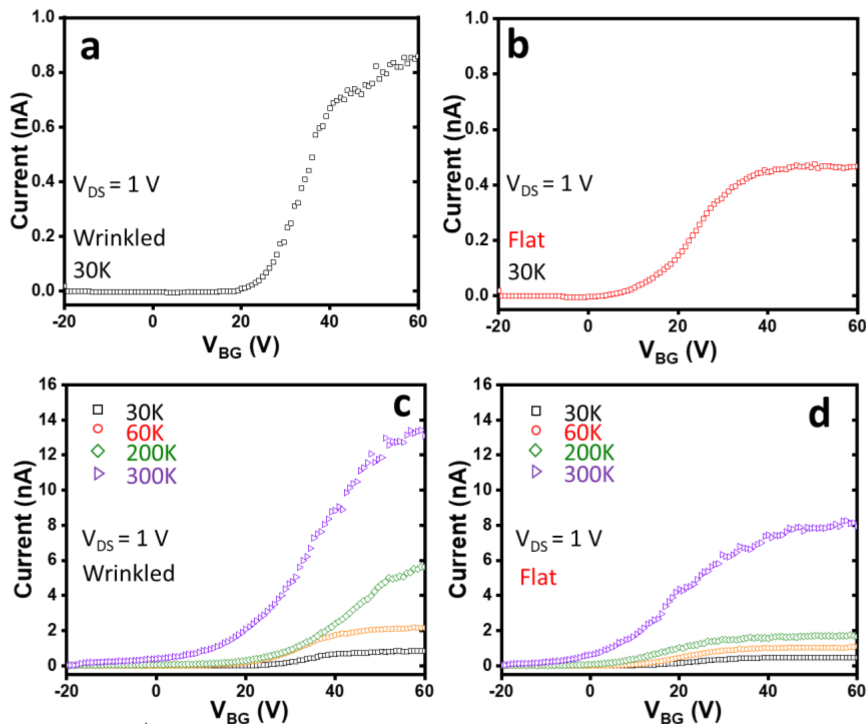

Figure S15. I_{DS}-V_{BG} (source-drain current versus back gating voltage) characterization and temperature studies of single-wrinkle and flat MoS_2 devices. (a) and (b) I_{DS} versus V_{BG} at 30K for wrinkled and flat MoS_2 devices, respectively. Insert is the optical image of tested device and the scale bar is 10 µm. (c) and (d) I_{DS} in linear scale versus V_{BG} at different temperatures for wrinkled and flat MoS_2 devices, respectively.

TRANSPORT BARRIERS CALCULATION

To determine the transport-barrier, the temperature dependence of the electrical conductivity at different gate voltages was analyzed (Figure 3h and 3i). The conduction behavior was found to be different for high temperature (200 to 300 K) and low temperature (15 to 200 K) ranges (Figure 3h and 3i). This is because at high temperature the charge transport is thermally activated and at low temperature the transport is dominated by hopping of localized states.[37,38] The activation energy

($G \propto exp(\frac{E_A}{kT})$) ($G$ is conductance, E_A is the activation energy and kT is the thermal energy) was 162.1 meV and 153.6 meV (at $V_{DS} = 0\ V$) for the wrinkled and flat MoS_2 devices at high temperature range (200 to 300 K), respectively. This indicates a >8 meV increase of barrier for the in-plane carrier-flow across the MoS_2 wrinkle.

Table S3 Transport barriers in temperature study

T	1/kT	Ln(R$_F$)	T	1/kT	Ln(R$_W$)
K	**(eV)$^{-1}$**		**K**	**(eV)$^{-1}$**	
60	193.4087086	25.98119926	80	145.0565314	23.62627652
100	116.0452251	25.24123945	100	116.0452251	
150	77.36348343	24.46831722	150	77.36348343	23.10884118
200	58.02261257	23.82757129	200	58.02261257	23.19022309
250	46.41809006	22.55733813	250	46.41809006	22.26135353
300	38.68174172	20.78403305	300	38.68174172	19.91942811

We have:

$$Ln(R) \propto (\frac{E_A}{kT}) \quad (2)$$

Based on the slopes of $Ln(R) \propto (\frac{1}{kT})$ plots at high temperature regions (200 to 300 K), we can have the transport barriers of two kinds of devices.

Additional Devices Characterization (wrinkled and flat devices on DIFFERENT flakes)

Note: The different colors in optical images are due to changes of contrast set-up in optical microscope, as shown the different gold electrodes color

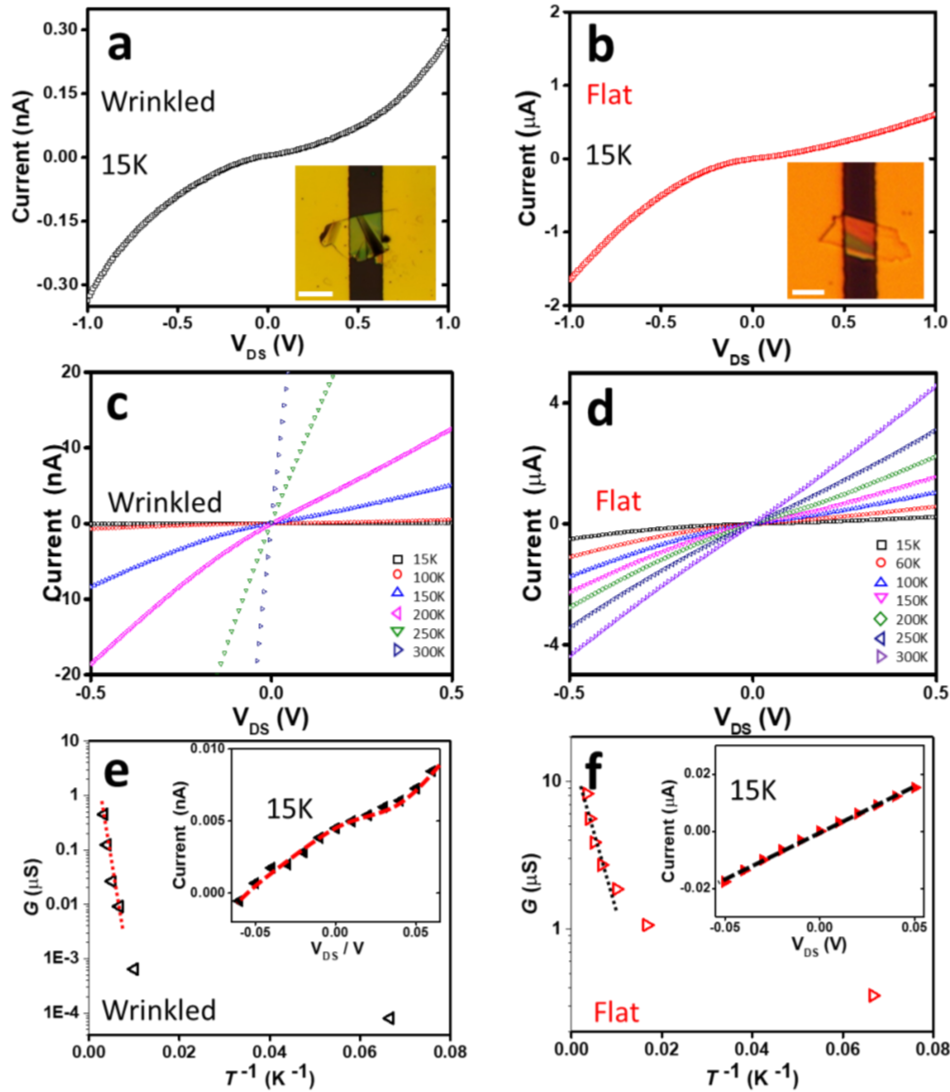

Figure S16. I_{DS}-V_{DS} characterization and temperature study of wrinkled and flat MoS_2 devices. (a) and (b) Source-drain current (I_{DS}) versus source-drain voltage (V_{DS}) at 15K. Inserts are optical images of single wrinkled and flat MoS_2 devices, scale bars are 20 mm. (c) and (d) Source-drain current (I_{DS}) versus source-drain voltage (V_{DS}) at different temperatures for wrinkled and flat MoS_2 devices, respectively. (e) and (f) Active energy studies of wrinkled and flat MoS_2 devices, respectively. The inserts are the typical I_{DS} versus V_{DS} at 15K for wrinkled and flat MoS_2 devices, respectively.

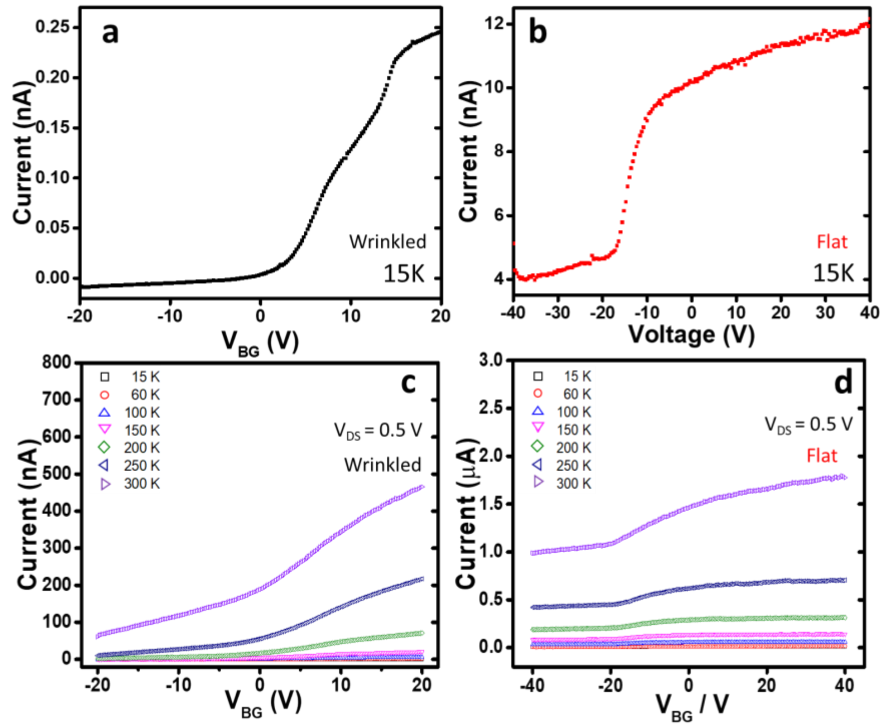

Figure S17. I_{DS}-V_{BG} characterization and temperature studies of wrinkled and flat MoS_2 devices. (a) and (b) Source-drain current (I_{DS}) versus back gating voltage (VDS) at 15 K for wrinkled and flat MoS2 devices, respectively. (c) and (d) Source-drain current (I_{DS}) in linear scale versus back gating voltage (V_{BG}) at different temperatures for wrinkled and flat MoS_2 devices, respectively.

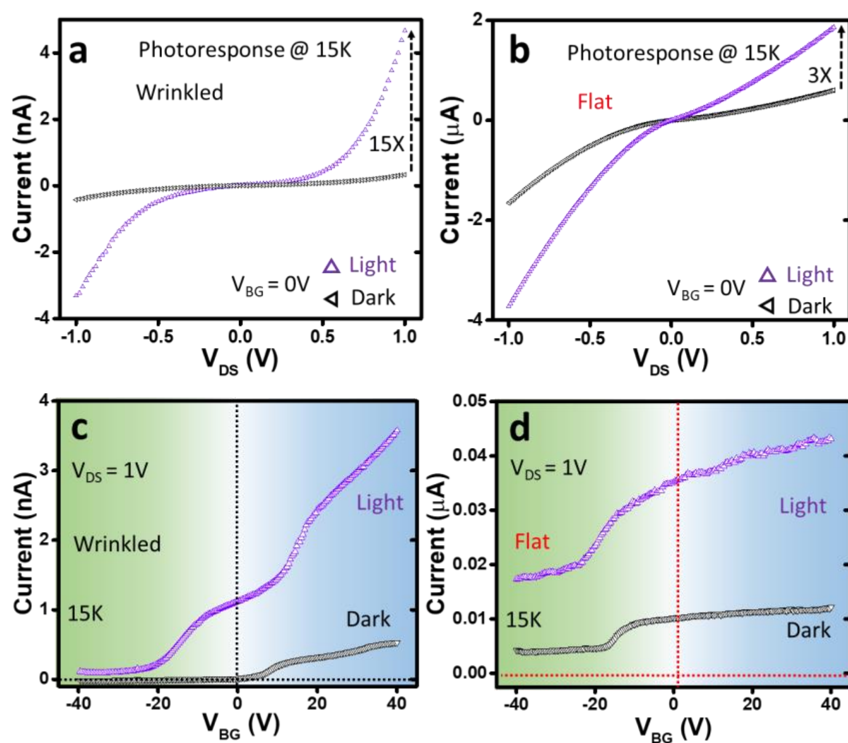

Figure S18. Photo-response studies of wrinkled and flat MoS_2 devices. (a) and (b) Photo-response studies of wrinkled and flat MoS_2 devices without gating at 15 K, respectively. (c) and (d) Typical source-drain current (I_{DS}) versus back gating voltage (V_{DS}) at 15 K for wrinkled and flat MoS_2 devices, respectively.

MOBILITY CALCULATION:

The mobility data at $V_{DS} = 1V$ and $V_{BG} = 0V$ at 300K in Figure 3 of the main text was applied.

The mobility in flat MoS_2:

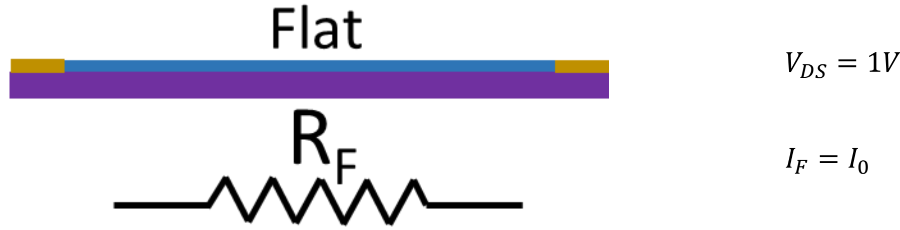

$V_{DS} = 1V$

$I_F = I_0$

The back gated field-effect mobility of these MoS_2 devices can be estimated based on the equation:[5]

$$\mu = \frac{L}{W\left(\frac{\varepsilon_r \varepsilon_0}{D}\right) V_{DS}} \frac{dI_{DS}}{dV_{BG}} \tag{3}$$

Where, L and W are the length and width of MoS_2 channel, respectively; ε_r is relative permittivity and ε_0 is vacuum permittivity (8.854×10^{-12} F·m^{-1}), and D is the gate-oxide thickness. There are two dielectric layers in series (285 nm of SiO_2 and an layer of air) in wrinkled part of MoS_2.

The mobility in flat devices:

$$\mu_F = \frac{L}{W\left(\frac{\varepsilon_{sio2}\varepsilon_0}{D}\right) V_{DS}} \frac{dI_{DS}}{dV_{BG}} = \frac{3}{10\left(\frac{3.9 \times 8.854 \times 10^{-12}}{285 \times 10^{-9}}\right)1} \times 0.142 \times 10^{-6} \times 10^{4}$$

$$= 3.516 \ \mathrm{cm^2 V^{-1} S^{-1}}$$

Devices (Flat)	L/W	dI/dV(A/V)	V_{DS}(V)	Mobility ($cm^2V^{-1}S^{-1}$)
1	0.3	1.42E-07	1	3.516
2	0.3	2.6905E-08	1	0.666
3	1.6	9.8882E-09	1	1.306
4	1.6	1.5399E-09	1	0.203

The mobility in wrinkled MoS_2:

The resistant of flat parts (R_{F1} and R_{F2}) in wrinkled device compared to the resistance of flat device:

$$R = \frac{L}{ne\mu A} \tag{4}$$

Assume the flat parts of MoS_2 and MoS_2 in flat devices have same (n, μ and A), also $L_{F1} + L_{F2} = 0.66\ L_F$, so we have:

$$\frac{R_{F1} + R_{F2}}{R_F} = \frac{0.66}{1}$$

Combine the current relationship in two kinds of devices ($I_F = 10 I_W$ under $V_{DS} = 1V$ and $V_{BG} = 0V$ at 30K), so the voltage drops of wrinkled part (R_W) is: $\Delta V_W = V_{DS} - 0.66 \times 0.1 = 0.934V$;

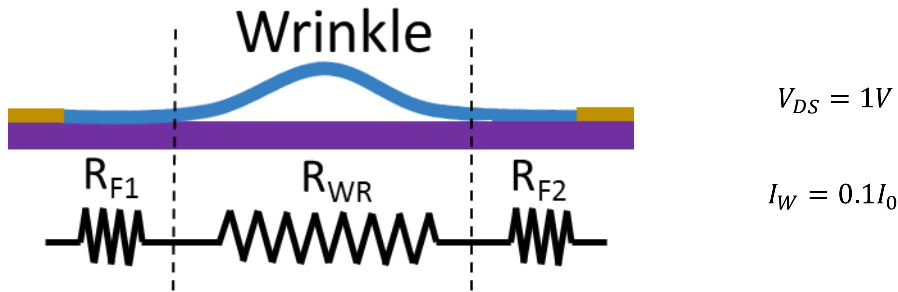

$$V_{DS} = 1V$$

$$I_W = 0.1 I_0$$

We can apply different a model to calculate the capacitance of the gate in the wrinkled MoS_2 devices:

Considering the wrinkled MoS_2 as a cylinder on a conducting plate:[6,7]

$$\mu_W = \frac{2 L_W W}{\Delta V_W C_g} \frac{dI_{DS}}{dV_{BG}}$$

Where L_W is the length of the wrinkle, and $2L_W$ is the wrinkled affect length, W is the width of the channel, C_g is the capacitance of the gate.

Back gate capacitance per unit length in this cylinder on a plate model:

$$\frac{C_g}{W} = \frac{2\pi\varepsilon_{ox}\varepsilon_0}{cosh^{-1}(\frac{r+h}{r})}$$

where r is the wrinkles radius (25 nm), h is the SiO_2 thickness (285 nm), and ε_{ox} is the SiO_2 dielectric constant (ε_{ox}= 3.9).

$$\text{so: } \mu_W = \frac{L_W}{\Delta V_W \frac{2\pi\varepsilon_{ox}\varepsilon_0}{cosh^{-1}(\frac{r+h}{r})}} \frac{dI_{DS}}{dV_{BG}} = \frac{0.8\times10^{-6}}{0.934\times\frac{2\pi\times3.9\times8.854\times10^{-12}}{cosh^{-1}(\frac{25+285}{25})}} \times 0.151\times10^{-6}\times10^{4} = 19.131\ \mathrm{cm^2V^{-1}S^{-1}}$$

Devices (Wrinkled)	L (m)	dI/dV(A/V)	V_{DS}(V)	Mobility ($cm^2V^{-1}S^{-1}$)
1	8E-07	1.51E-07	0.934	19.131
2	7E-07	9.6672E-09	0.934	1.072
3	1.2E-06	9.1193E-09	0.98	1.652
4	1.2E-06	1.8761E-09	0.98	0.340

Table S4 Mobilities of flat and wrinkled devices

	Mobility ($cm^2V^{-1}S^{-1}$)	
Devices	Flat	Wrinkled
1	0.67	1.07
2	1.31	1.65
3	0.20	0.34
4	3.52	19.13
Average	1.42	5.55

$\mu_W \approx 3.9\ \mu_F$

We apply $\mu_W = x\mu_F$ in the following calculations and demonstrations.

Doping Concentration:

$$R = \frac{L}{ne\mu A}$$

$$\mu_W \approx x\mu_F$$

$$\frac{R_F}{R_W} = \frac{\frac{L_F}{n_F}}{\frac{L_{F1} + L_{F2}}{n_F} + \frac{L_{WR}}{xn_{WR}}} \approx \frac{1}{10}$$

With $L_F = 5\ L_W$

$$\frac{\frac{3}{n_F}}{\frac{2}{n_F} + \frac{1}{xn_{WR}}} = \frac{1}{10}$$

$$x \approx \ 3.9$$

$$n_F = 13x\ n_{WR} = \ 50.7\ n_{WR}$$

$n_F \approx 10^{13}$ cm^{-2}

So $n_{WR} \approx 1.97 \times 10^{11}$

Fresnel Effect at Wrinkled Flakes

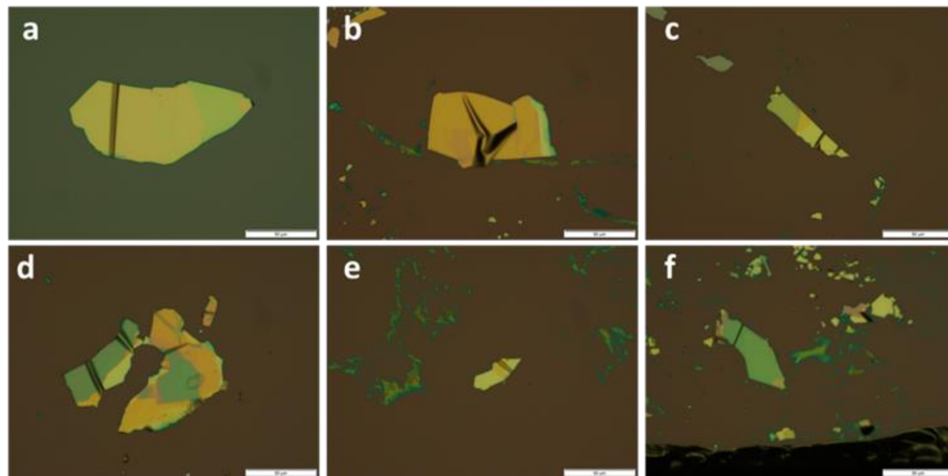

Figure S19. Examples of Fresnel effect on wrinkled part of MoS_2. Scale bars are 50μm.

For non-magnetic media, Fresnel equations have forms for reflectance of s-polarized light and p-polarized lights:

$$R_s = \left| \frac{n_1 cos\theta_i - n_2\sqrt{1-\left(\frac{n_1}{n_2} sin\theta_i\right)^2}}{n_1 cos\theta_i + n_2\sqrt{1-\left(\frac{n_1}{n_2} sin\theta_i\right)^2}} \right|^2 \quad \text{(S2)}$$

$$R_p = \left| \frac{n_1\sqrt{1-\left(\frac{n_1}{n_2} sin\theta_i\right)^2} - n_2 cos\theta_i}{n_1\sqrt{1-\left(\frac{n_1}{n_2} sin\theta_i\right)^2} + n_2 cos\theta_i} \right|^2 \quad \text{(S3)}$$

Based on these two equations, we can plot the reflectance at air/MoS_2 interface as function of angle of incidence as shown in Figure 13a.

Table S5. Reflectance at air/MoS_2 interface (light from air to MoS_2)

Reflective index[3,4] of air and MoS_2: Air $n_1 = 1$ and MoS2 $n_2 = 4$

Angles/°	0	10	20	30	40	50	60	70	80	90
Rs	0.36	0.3655	0.3825	0.4121	0.4563	0.5175	0.5993	0.7054	0.8397	1.0053
Rp	0.36	0.3544	0.3373	0.3073	0.2621	0.1990	0.1165	0.0268	0.0316	1.0891

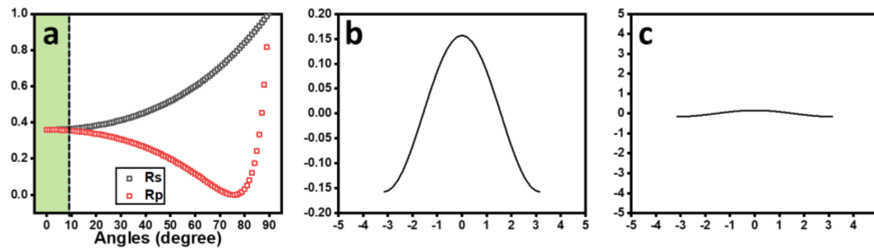

Figure S20. Reflectance of at air/MoS_2 interface and sine function model of a single wrinkle structure. (a) Reflectance of at air/MoS_2 interface based on equation S2 and S3, light propagates

from air to MoS_2 with incidence angle θ_i. (b) and (c) Sine function model of a typical wrinkle in MoS_2 at different y axial scale.

Based on the AFM data, most wrinkles have an aspect ratio (amplitude/width $\frac{A}{W}$) less than 0.05 and the wrinkle's contour can be modeled with the function $y = 0.157\sin(x + 1.57)$, as shown in Figure S13b. The actual shape of the wrinkle is clearly shown as plotting it with x and y axials in the same scale (Figure S13c). The maxmium incident angles is arcsin $(\pm 0.157) = 9.03°$ at $x = \pm 1.57$. Further, as shown in Figure 13a, the reflectances are close to constant when angles of incidence are smaller than 10°. The amount of transmittance of the lights $\mathrm{T} = 1 - \mathrm{R}$ is also constant within the 0 to 9.03° range of incident angles, as shown in the green zone in Figure 13a. Therefore, the Fresnel effect does not obviously enhance the light absoption at the wrinkle regions.

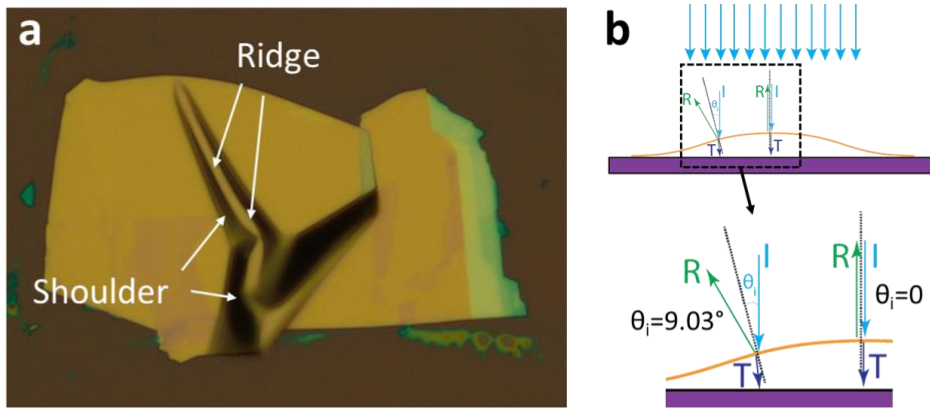

Figure S21. Fresnel effect on wrinkled MoS_2 flake. (a) Schematic side view of the Fresnel effect on single wrinkled MoS_2. Blue arrows are the incident lights, green arrow are reflective lights, dark blue arrows are transmitted lights, and black dashed line is the normal of the left shoulder. (b) Bright ridges and dark shoulders on a wrinkled MoS_2.

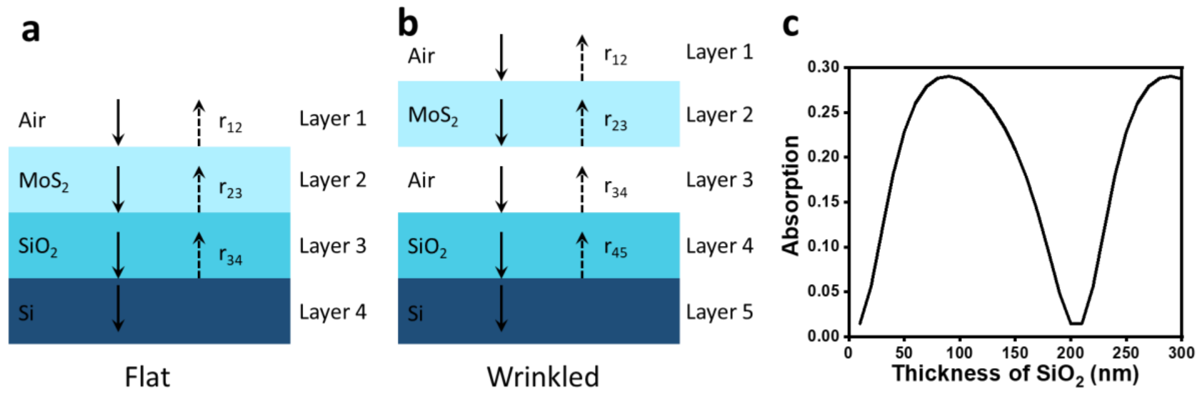

Figure S22. Multilayer models and absorption of flat MoS_2 at different thickness of SiO_2. Schematic illustration of multilayer model of wrinkled MoS2 device. (b) absorption of wrinkled MoS2 at different thickness of SiO2. (c) Individual Energy band diagram of individual flat and wrinkled MoS2; (d) device at no bias; and (e) wrinkled MoS2 device under bias voltage. Blue and green spheres are electrons and holes, respectively. The filled arrows are the directions of carriers' moving and the unfilled arrows represent the current directions (IDS). Multilayer modes of flat (a) and single-wrinkle (b) MoS_2. (c) Absorption of flat MoS_2 at different thickness of SiO_2 on silicon.

Table S6 Absorption of wrinkled MoS_2 at different thickness of air gap

Thickness/nm	Absorption	Thickness/nm	Absorption	Thickness/nm	Absorption
0	0.2901	36	0.2962	72	0.281
3	0.2917	39	0.2957	75	0.2789
6	0.293	42	0.295	78	0.2767
9	0.2941	45	0.2942	81	0.2743
12	0.295	48	0.2933	84	0.2717
15	0.2958	51	0.2922	87	0.269
18	0.2963	54	0.291	90	0.2662
21	0.2967	57	0.2897	93	0.2632
24	0.2969	60	0.2882	96	0.2601
27	0.297	63	0.2866	99	0.2568
30	0.2969	66	0.2849	102	0.2533

Table S7 Absorption of flat MoS_2 at different thickness of SiO_2

Thickness/nm	Absorption	Thickness/nm	Absorption	Thickness/nm	Absorption
10	0.0146	110	0.2801	210	0.0146
20	0.0558	120	0.2688	220	0.0558
30	0.1197	130	0.2534	230	0.1197
40	0.1816	140	0.2336	240	0.1816
50	0.229	150	0.2087	250	0.229
60	0.2605	160	0.1775	260	0.2605
70	0.2791	170	0.1391	270	0.2791
80	0.2883	180	0.0941	280	0.2883
90	0.2905	190	0.0475	290	0.2905
100	0.2875	200	0.0142	300	0.2875

References in Electronic Supplementary Information

1 D. Lloyd, X. Liu, J. W. Christopher, L. Cantley, A. Wadehra, B. L. Kim, B. B. Goldberg, A. K. Swan and J. S. Bunch, *Nano Lett.*, 2016, **16**, 5836–5841.

2 S. Deng, E. Gao, Z. Xu and V. Berry, *ACS Appl. Mater. Interfaces*, 2017, **9**, 7812–7818.

3 H. Zhang, Y. Ma, Y. Wan, X. Rong, Z. Xie, W. Wang and L. Dai, *Sci. Rep.*, 2015, **5**, 8440.

4 A. R. B. and H. P. Hughes, *J. Phys. C Solid State Phys.*, 1979, **12**, 881.

5 Z. Yin, H. Li, H. Li, L. Jiang, Y. Shi, Y. Sun, G. Lu, Q. Zhang, X. Chen and H. Zhang, *ACS Nano*, 2012, **6**, 74–80.

6 E. Lind, A. I. Persson, L. Samuelson and L.-E. Wernersson, *Nano Lett.*, 2006, **6**, 1842–1846.

7 D. R. Khanal and J. Wu, *Nano Lett.*, 2007, **7**, 2778–2783.